



HAL
open science

Topoisomerase VI participates in an insulator-like function that prevents H3K9me2 spreading

Louis-Valentin Meteignier, Cécile Lecampion, Florent Velay, Cécile Vriet, Laura Dimnet, Martin Rougée, Christian Breuer, Ludivine Soubigou-Tacconnat, Keiko Sugimoto, Fredy Barneche, et al.

► To cite this version:

Louis-Valentin Meteignier, Cécile Lecampion, Florent Velay, Cécile Vriet, Laura Dimnet, et al.. Topoisomerase VI participates in an insulator-like function that prevents H3K9me2 spreading. Proceedings of the National Academy of Sciences of the United States of America, 2022, 119 (27), 10.1073/pnas.2001290119 . hal-03862125

HAL Id: hal-03862125

<https://cnrs.hal.science/hal-03862125>

Submitted on 28 Nov 2022

HAL is a multi-disciplinary open access archive for the deposit and dissemination of scientific research documents, whether they are published or not. The documents may come from teaching and research institutions in France or abroad, or from public or private research centers.

L'archive ouverte pluridisciplinaire **HAL**, est destinée au dépôt et à la diffusion de documents scientifiques de niveau recherche, publiés ou non, émanant des établissements d'enseignement et de recherche français ou étrangers, des laboratoires publics ou privés.



Distributed under a Creative Commons Attribution - NonCommercial - NoDerivatives 4.0 International License

1 **Topoisomerase VI participates in an insulator-like function that prevents H3K9me2**
2 **spreading.**

3

4 Louis-Valentin Méteignier¹, Cécile Lecampion¹, Florent Velay¹, Cécile Vriet^{1,2}, Laura Dimnet¹, Michel
5 Térése³, Martin Rougée^{4,5}, Christian Breuer⁶, Ludivine Soubigou-Taconnat^{7,8}, Keiko Sugimoto⁶, Fredy
6 Barneche^{4,5} and Christophe Laloi^{1*}.

7

8 ¹Aix Marseille Univ, CEA, CNRS, BIAM, Marseille, France F-13009

9 ²UMR CNRS 7267, University of Poitiers, 86073 Poitiers Cedex

10 ³Independent informatician, 06100 Nice, France

11 ⁴IBENS, Département de Biologie, Ecole Normale Supérieure, CNRS, PSL Research University, F-
12 75005, Paris, France

13 ⁵Université Paris-Sud, Université Paris-Saclay, 91405, Orsay, France.

14 ⁶RIKEN Center for Sustainable Resource Science, Yokohama, 230-0045, Japan

15 ⁷Institute of Plant Sciences Paris Saclay IPS2, CNRS, INRA, Université Paris-Sud, Université Evry,
16 Université Paris-Saclay, Bâtiment 630, 91405 Orsay, France.

17 ⁸Institute of Plant Sciences Paris-Saclay IPS2, Paris Diderot, Sorbonne Paris-Cité, Bâtiment 630,
18 91405, Orsay, France

19

20 **Corresponding author:**

21 Christophe Laloi, christophe.laloi@univ-amu.fr

22

23 **Classification:**

24 BIOLOGICAL SCIENCES: Plant Biology

25

26 **Keywords**

27 Euchromatin islands / Heterochromatin spreading / Insulator / Methionine Adenosyltransferase /
28 Topoisomerase VI.

29

30 **Abstract**

31 The organization of the genome into transcriptionally active and inactive chromatin domains requires
32 well-delineated chromatin boundaries and insulator functions in order to maintain the identity of
33 adjacent genomic loci with antagonistic chromatin marks and functionality. In plants that lack known
34 chromatin insulators, the mechanisms that prevent heterochromatin spreading into euchromatin
35 remain to be identified. Here, we show that DNA Topoisomerase VI participates in a chromatin
36 boundary function that safeguards the expression of genes in euchromatin islands within silenced
37 heterochromatin regions. While some transposable elements are reactivated in mutants of the
38 Topoisomerase VI complex, genes insulated in euchromatin islands within heterochromatic regions
39 of the *Arabidopsis thaliana* genome are specifically downregulated. H3K9me2 levels consistently
40 increase at euchromatin island loci and decrease at some TE loci. We further show that
41 Topoisomerase VI physically interacts with S-adenosylmethionine (SAM) synthase MAT3, which is
42 required for H3K9me2. A Topoisomerase VI defect affects MAT3 occupancy on heterochromatic
43 elements and its exclusion from euchromatic islands, thereby providing a possible mechanistic
44 explanation to the essential role of Topoisomerase VI in the delimitation of chromatin domains.

45

46 **Significance Statement**

47 In the eukaryotic genome, DNA associates with proteins and form two main types of chromatin, the
48 highly condensed heterochromatin, which is inaccessible to transcription factors and hence
49 transcriptionally silent, and the less condensed, hence transcriptionally active euchromatin. The
50 maintenance of sharp boundaries between these chromatin domains with antagonistic functionality
51 is therefore critical for transcriptional control and involves chromatin insulators that remain
52 unknown in plants. Here, we show that a plant topoisomerase participates in such a chromatin
53 boundary function that prevent heterochromatin spreading into euchromatin and hence safeguards
54 the expression of genes in euchromatin islands within silenced heterochromatin regions. We have
55 also identified partners of this topoisomerase that allow us to provide a mechanistic insight to this
56 insulator-like function.

57

58 Introduction

59 The discovery of position effect variegation in *Drosophila melanogaster* paved the way
60 towards revealing the importance of chromatin contexts in the regulation of gene expression (1, 2).
61 Since then, cytogenetic and molecular profiling of the epigenome, as well as topological analyses of
62 chromatin architecture, have allowed the mechanisms involved in partitioning the gene-rich
63 euchromatic fraction from the repeat-rich heterochromatic fraction to be elucidated. Large protein
64 complexes specific to insulator DNA sequences contribute to partitioning chromatin domains with
65 distinct identity at multiple scales. These complexes maintain the identity of adjacent genomic loci
66 with antagonistic chromatin marks and functionality, and more globally influence the formation of
67 long-range chromosomal interactions (3). Insulator binding proteins such as the CCCTC-binding factor
68 CTCF, BEAF-32, CP190 and Mod have been best described in *Drosophila* where they play critical roles
69 in the definition of chromatin and transcriptional status. In vertebrates, CTCF is the only known
70 insulator binding protein homologue. CTCF is enriched at insulator DNA sequences that define large
71 topological domains of the genome (4–6) and, in some cases, define boundaries between adjacent
72 chromatin domains with distinct features (7). Surprisingly, CTCF orthologs cannot be identified in
73 many eukaryotic organisms, including plants (8). Moreover, very few studies support the presence of
74 insulator DNA sequences or insulator-like regions in plants (9–11), and insulator binding factors
75 remain to be identified. This contrasts with the observation that *Arabidopsis thaliana* and other plant
76 species display highly indexed chromatin states along the genome, with well-defined chromatin
77 signatures around transcriptionally active or repressed genes, as well as close relationships between
78 chromatin composition and genome topology in the nuclear space (12, 13). In *Arabidopsis*,
79 heterochromatin is found on hundreds of transposable elements (TEs) mostly confined within the
80 pericentromeric regions and at a few knob structures that tend to associate through long-distance
81 interactions in the nuclear space (14–18). As a result, in *Arabidopsis* interphase nuclei most
82 cytologically visible heterochromatin is condensed within 8 to 10 conspicuous foci that are referred
83 to as chromocenters (19–21). Consistent with their heterochromatic nature, chromocenters are
84 refractory to transcription and contain highly methylated DNA (22) as well as histone modifications
85 such as H3K9me2 and H3K27me2 (23, 24). Nonetheless, many expressed genes exhibiting
86 euchromatic features appear to be located in close vicinity to large heterochromatic regions in the
87 *Arabidopsis* genome, notably within the pericentromeric and knob regions (25, 26). The mechanisms
88 by which gene-containing euchromatic islands (EIs) are insulated from neighboring heterochromatin
89 regions and how their transcriptional capacities are preserved in such chromatin contexts are largely
90 unknown. In this study, we have unveiled an essential function of the plant Topoisomerase VI
91 complex in preserving the functional and structural identity of EIs.

92 DNA topoisomerases are enzymes that introduce transient DNA breaks to resolve topological
93 constraints that arise during multiple cellular processes such as replication, transcription,
94 recombination and chromatin remodeling. The plant Topo VI, a type II topoisomerase first identified
95 in the archaeon *Sulfolobus shibatae* (27, 28), was initially implicated in various biological processes
96 involving endoreduplication, such as root hair growth (29–31), hypocotyl elongation (31) and nodule
97 differentiation (32). Topo VI forms an A₂B₂ heterotetramer whose A and B subunits are encoded by
98 single genes in *Arabidopsis*, *AtTOP6A/CAA39/AtSPO11-3/RHL2/BIN5/AT5G02820* and
99 *AtTOP6B/RHL3/BIN3/HYP6/HLQ/AT3G20780*, respectively (33–37). Two additional subunits named
100 ROOT HAIRLESS 1 (RHL1/HYP7/AT1G48380) and BRASSINOSTEROID-INSENSITIVE 4
101 (BIN4/MID/AT5G24630) (31, 38, 39) are essential for the *Arabidopsis* Topo VI function and appear to
102 be evolutionarily conserved in plants and in other eukaryote groups, whilst their precise functions
103 remain unclear. However, BIN4 shares sequence similarity with the C-terminal region of animal Topo
104 II α , which seems to have regulatory functions (40–42), and exhibits stable DNA binding *in vitro* (38).
105 Therefore, it has been proposed that BIN4 may have a regulatory role in the plant Topo VI complex,
106 presumably by holding the substrate DNA through its AT-hook motif (38, 39).

107 In recent years, evidence has accumulated that topoisomerases have more diverse and
108 specialized functions than previously thought (43). In particular, transcriptomic analyses of several
109 Topo VI mutants revealed that Topo VI influences the expression of many nuclear genes, including
110 genes regulated by phytohormones (35, 36) or by reactive oxygen species (44–46). A function of
111 *Arabidopsis* Topo VI as a chromatin-remodeling complex has also been speculated (35). This
112 hypothesis has since been supported by the observation that loss of the Topo VI B subunit in *hlq*
113 mutant plants leads to the mis-expression of numerous adjacent genes, hence possibly triggering
114 positional or chromatin context dependent transcriptional defects (36). This is further supported by
115 the implication of the BIN4 subunit in heterochromatin organization, as observed by smaller and
116 diffuse chromocenters in interphase nuclei of plants bearing the severe *mid* mutation (39).

117 Here, we reveal that *Arabidopsis* Topo VI is required for chromocenter formation and for
118 efficient silencing of some heterochromatic TEs but has an antagonistic effect on genes localized in
119 euchromatic islands (EIs). Downregulation of EI genes in Topo VI mutant plants is associated with an
120 enrichment of the H3K9me2 heterochromatic mark. We further report that the BIN4 subunit of Topo
121 VI directly interacts with S-adenosylmethionine (SAM) synthetase 3 / Methionine Adenosyl
122 transferase 3 (MAT3). Similar to Topo VI knockdown plants, *mat3* knockdown mutants exhibit de-
123 repression of heterochromatic TEs and a decrease in H3K9me2. Furthermore, we show that the
124 association of MAT with heterochromatic elements is reduced in a hypomorphic Topo VI mutant,
125 whereas it increased at some EIs. We therefore propose that Topo VI has a prominent role in the

126 delimitation of chromatin boundaries, could participate in defining SAM synthesis sites onto specific
127 regions of the genome, and collectively has an essential role in the establishment of distinct
128 chromatin domains.

129

130 **Results**

131 **Topoisomerase VI is required for heterochromatin organization**

132 Kirik *et al.* reported that interphase nuclei of the severe *mid* mutant in the BIN4/MID subunit
133 presents smaller and less defined chromocenters (CCs) compared to the wild-type (wt), suggesting
134 that heterochromatin organization is affected by the *mid* mutation (39). However, this phenotype
135 was not reported in the allelic *bin4-1* mutant, which also has a severe phenotype (38). Therefore, to
136 unequivocally confirm the role of the *Arabidopsis* Topo VI complex in nuclear organization, we
137 analyzed the nuclear phenotypes of hypomorphic and amorphic mutants of the AtTOP6A subunit,
138 *caa39* and *rhl2-1*, and of the BIN4/MID subunit, a *BIN4* knockdown line (*BIN4* KD, see below) and
139 *bin4-1*, by DAPI DNA staining and immunolocalization of heterochromatin hallmarks. Both the *caa39*
140 and *rhl2-1* mutants exhibited strong alterations in heterochromatin organization with largely
141 decondensed chromocenters (Fig 1A, top panel, and SI Appendix, Fig S1A). Likewise, nuclei of
142 epidermal and mesophyll cotyledon cells from *BIN4* KD and *bin4-1* did not harbor conspicuous
143 chromocenters (SI Appendix, Fig S1A), as previously reported for the *mid* allelic mutants (39). In
144 contrast, the nuclear phenotype of shoot apical meristematic cells is similar in wt, *caa39*, *rhl2-1*,
145 *bin4-1* and *BIN4* KD lines, with equal proportions of nuclei with conspicuous (type 1) or diffuse (type
146 2) chromocenter profiles (SI Appendix, Fig S1A, meristem panel, and Fig S1B). Consistent with its role
147 in endocycles but not in mitosis (31, 37–39), these defects indicate that Topo VI is required for
148 chromatin organization of differentiated cells, but less of actively dividing cells. Immunofluorescence
149 analysis of the heterochromatin hallmark H3K9me2 confirmed the large extent of heterochromatin
150 decondensation in *caa39* Topo VI mutant plants (Fig 1A). Immunoblot analyses further showed that
151 the global level of H3K9me2 is not affected in *caa39* seedlings (Fig 1B). Likewise, 5-methylcytosine (5-
152 meC) immunolabeling also revealed a dispersed signal in *caa39* nuclei (Fig 1C) whereas an anti-5-meC
153 ELISA showed overall similar levels of 5-meC in wt and *caa39* as compared to *ddm1-8* seedlings (Fig
154 1D). These results suggest that the marked alteration of chromocenter morphology does not result
155 from a global decrease in heterochromatin hallmarks in *caa39*.

156

157 **Topo VI is required for the silencing of heterochromatic transposable elements**

158 A role for *Arabidopsis* Topo VI in heterochromatin-dependent transcriptional gene silencing
159 was highlighted by the reactivation of *TRANSCRIPTIONALLY SILENT INFORMATION (TSI)* in *mid* mutant
160 plants (39). However, reactivation was not observed in the *bin4-1* allelic mutant (38). Therefore, to
161 unambiguously assess the involvement of Topo VI in transcriptional silencing and get a more global
162 understanding of Topo VI influence on TE repression, we performed a RNA-seq analysis of *caa39* and
163 wt transcripts. Multiple heterochromatic TEs (176 TEs with $\log_2(\text{FC}) > 2$), particularly from the
164 LTR/Gypsy, LTR/Copia and En-Spm/CACTA superfamilies (47), are reactivated in *caa39* plants (Fig 2A,
165 Dataset S1). Conversely, 91 TEs are repressed in *caa39* ($\log_2(\text{FC}) < -2$); unlike reactivated TEs, these
166 repressed TEs are rarely in the most inaccessible and repressive heterochromatin state 9 (SI
167 Appendix, Fig S2A). To test for TE silencing defects in other Topo VI mutants, we selected several de-
168 repressed heterochromatic TEs loci (Dataset S1) for which robust primer design was feasible, and
169 measured their relative transcript abundance by RT-qPCR in *rh12-1* and *bin4-1* mutants along with the
170 *caa39* and wt lines. A clear increase in TE transcript abundance was observed for all three tested
171 Topo VI mutant lines (Fig 2B).

172 Although we found no global decrease of H3K9me2 and 5-meC in *caa39* (Fig 1B and 1D),
173 more subtle local changes could account for TE reactivation. We first assessed DNA methylation
174 levels at individual TEs in Topo VI mutants as compared to wt and *ddm1-8* plants by digestion with
175 the methylation-dependent restriction enzyme McrBC. As expected, very efficient digestion of TEs
176 was observed in wt but not in *ddm1-8* plants, reflecting a nearly complete loss of DNA methylation
177 over multiple TEs in this hypomethylated mutant line (Fig 2C). In sharp contrast, we observed wt
178 levels of DNA methylation for all tested loci in *caa39* and *bin4-1* plants. This trend was confirmed in
179 different sequence contexts (CG, CHG and CHH) by using the methylation-sensitive restriction
180 enzymes HpaII, MspI and HaeIII (SI Appendix, Fig S3). Similar DNA methylation levels of TEs in wt and
181 *caa39* were then confirmed genome-wide by whole-genome bisulfite sequencing, in all three
182 contexts (Fig 2D). We concluded that TE de-repression in Topo VI mutants could not be accounted for
183 by a global decrease of DNA methylation in *cis*. Next, we measured the level of H3K9me2 at TEs,
184 which could be performed only with the *caa39* hypomorphic mutant, owing to the extreme dwarf
185 phenotype of the *rh12-1* and *bin4-1* null mutants. ChIP-qPCR analyses revealed a modest decrease in
186 H3K9me2 at some but not all tested TEs in *caa39* as compared to wt plants (Fig 2E). ChIP-seq analysis
187 of H3K9me2 levels in wt and *caa39*, normalized to H3 levels in each line, confirmed the slight
188 decrease of H3K9me2 at *AT3TE60425* and *AT4TE15030*, but not at *AT2TE15415* and *AT4TE16900* (SI
189 Appendix, Fig S2B-C), and revealed a significant global decrease ($P < 0.01$, Mann-Whitney test) of
190 H3K9me2 at TEs (Fig 2F). Collectively, these results suggest that H3K9me2 local decreases and

191 heterochromatin spatial reorganization may contribute to TE activation, although the precise causal
192 mechanism is unknown.

193

194 **Unlike TEs, genes interspersed within pericentromeric and chromosome 4 knob large**
195 **heterochromatin regions are massively downregulated in Topo VI mutants**

196 We then used the online positional gene enrichment tool (48) to investigate the genomic
197 distribution of misregulated genes identified in our RNA-seq analysis of *caa39* (Dataset S2). This
198 analysis revealed that the 500 most downregulated genes are strikingly over-represented in
199 pericentromeric regions (PRs) and in the heterochromatic knob of chromosome 4 (*hk4S*, Fig 3A). In
200 these regions, 94% (181/193) of the non-TE genes that are differentially expressed in *caa39* are
201 downregulated (Dataset S2). In contrast, the 500 most highly upregulated genes displayed no
202 preferential localization (SI Appendix, Fig S4A). To determine whether this effect is robust in other
203 Topo VI mutant lines, we first examined the expression profiles of *bin4-1* and a second allelic mutant,
204 *bin4-2*, from microarray data that were generated during the initial characterization of these two
205 allelic lines (38). Despite the fact that *bin4-1* and *bin4-2* are knock-out mutants that have much more
206 severe developmental defects than *caa39*, and although two different technical platforms have been
207 used (RNA-seq for *caa39* vs Affymetrix ATH1 microarrays for *bin4-1* and *bin4-2*), we found a good
208 correlation between the different transcriptomes (SI Appendix, Fig S4B). In particular, 91% (72/79) of
209 the PR genes that are repressed in *caa39* and are detected in both RNA-seq and microarray
210 experiments are also downregulated in *bin4-1* or *bin4-2* (Fig 3B, Dataset S2). We examined further
211 the expression of seven pericentromeric genes distributed over the five chromosomes and strongly
212 repressed in *caa39*, by RT-qPCR in *caa39*, *bin4-1* as well as in *rhl2-1* plants. These genes were found
213 to be downregulated in all mutants, except for *AT4G06634* and *AT4G07390* that were not
214 significantly repressed in *rhl2-1* and *bin4-1* (Fig 3C). This could possibly be due to secondary effects of
215 the *bin4-1* and *rhl2-1* amorphic mutations as compared to the less severe *caa39* mutation. In order
216 to test this hypothesis, we took advantage of the availability of an *Arabidopsis* *BIN4* co-suppressed
217 transgenic line identified during the process of generating lines overexpressing *BIN4-CFP*. Rather than
218 exhibiting *BIN4* upregulation, this *BIN4* KD homozygous, mono-insertional transgenic line, shows
219 downregulation of *BIN4* (SI Appendix, Fig S5A-B) and develops a phenotype similar to *caa39* (SI
220 Appendix, Fig S5C). In this line, all tested pericentromeric genes were at least as much
221 downregulated as in *caa39*, with a more pronounced effect than in the *bin4-1* and *rhl2-1* knockout
222 mutants (Fig 3C). These observations indicate that Topoisomerase VI is required to maintain

223 transcriptional control of both genes and TEs in pericentromeric and *hk4S* regions, possibly acting as
224 a chromatin architectural factor.

225

226 **Downregulated genes within heterochromatic regions are localized in small euchromatic islands**

227 We then asked whether the inverse expression patterns of genes and TEs in pericentromeric
228 and *hk4S* regions in Topo VI mutants could be ascribed to their different chromatin landscapes. We
229 first inspected the individual chromatin landscape of the seven downregulated pericentromeric
230 genes confirmed by RT-qPCR (Fig 3C), using the nine chromatin states defined by Sequeira-Mendes *et*
231 *al.* (49). Euchromatin states 2, 1 and 3 characterize the proximal promoter, the transcriptional start
232 site, and the start of coding sequence, respectively. The intragenic states 6 and 7 are characteristic of
233 the transcriptional termination site and gene body of long transcribed genes, respectively. States 4
234 and 5 are highly enriched in H3K27me3 (a *Polycomb*-Repressive Complex 2 (PRC2)-based repressive
235 histone modification) and are usually found in intergenic regions and PRC2-targeted genes. Lastly,
236 the two types of heterochromatin states, 8 and 9, are enriched in H3K9me2, but in contrast with
237 state 8, state 9 preferentially defines pericentromeric heterochromatin and is devoid of H3K27me3
238 (49). Strikingly, all inspected loci share common features: a typical euchromatin context whose
239 proximal environment is composed of heterochromatic state 8 and whose distal environment is of
240 heterochromatic state 9 (SI Appendix, Fig S6A). Overall, these observations suggested that *caa39*
241 downregulated genes might be part of *bona fide* euchromatic islands (EIs).

242 To generate a comprehensive view of their structural features in the genome, we
243 systematically investigated the pericentromeric and *hk4S* heterochromatic regions defined in
244 Appendix Figure S6B. We designed a script to extract all EIs surrounded by chromatin states 8 and 9,
245 then we analyzed the proportion of chromatin states covering EIs and their 1.5 kb flanking regions
246 (Fig 3D). We identified 232 EIs containing 540 EI genes this way, among which 6 correspond to
247 unsequenced gaps (<https://jbrowse.arabidopsis.org/?data=Araport11>) and were discarded in
248 subsequent analyses (Dataset S3). Looking for EIs directly flanked by state 9 chromatin did not
249 increase the number of EIs identified, showing that chromatin state 8 is always present in the
250 proximal border (Fig 3D, SI Appendix, Fig S6C). In contrast, the number of detected EIs started to
251 decrease to 215 when considering two-nucleosome-long flanking regions in state 8, suggesting that
252 11 EIs have only one proximal nucleosome in state 8 (SI Appendix, Fig S6C). With respect to state 9,
253 the number of extracted islands began to drop from 4-nucleosome-long flanking regions, suggesting
254 that the state 8 proximal border is always flanked by at least 3-nucleosome-long state 9 regions (SI

255 Appendix, Fig S6C). A majority of EIs (157/232) are short and contain only one or two genes (Fig. 3E,
256 Dataset S3, SI Appendix, Table S1).

257

258 **Topo VI prevents the spreading of H3K9me2 into euchromatic islands**

259 Given the general repression of EI genes and the local decrease of H3K9me2 at some TE loci
260 without affecting the global level of H3K9me2 (Fig 1B), we hypothesized that EI gene repression
261 might result from ectopic spreading of this silencing mark over EIs. This was first tested on several EI
262 genes by ChIP-PCR analysis of H3K9me2 levels in wt and *caa39*. H3K9me2 levels were very low,
263 barely above background, in wt, consistent with the fairly high level of expression of these genes (Fig
264 4A). In contrast, a clear increase of H3K9me2 was observed in *caa39* (Fig 4A). Therefore, we further
265 tested the spreading of H3K9me2 over EIs on a genome-wide scale by ChIP-seq analysis of H3K9me2
266 levels in wt and *caa39*, normalized to H3 levels in each line. Analysis of the wt profile showed short
267 EIs (S-EIs, which contain only one or two genes and are < 6kb-long) with sharp boundaries and where
268 H3K9me2 was barely detected, flanked by regions with high H3K9me2 levels (Fig 4B). Consistent with
269 the minor decrease observed only on some TEs presented in Figure 2, the H3K9me2 level is globally
270 not lower in EI-flanking sequences in *caa39* as compared to wt. In contrast, a clear increase was
271 observed within S-EIs of *caa39*, which was highly significant all along S-EIs (Mann-Whitney test,
272 Benjamini-corrected $P < 0.01$), suggesting that Topo VI prevents H3K9me2 spreading across natural
273 boundaries (Fig 4B). H3K9me2 spreading into large and more complex EIs (L-EIs, > 6kb-long and often
274 containing internal state 8) was also highly significant and particularly pronounced on L-EIs
275 boundaries (Fig. 4C). Inspection of meta-profiles for each chromosome confirmed highly significant
276 H3K9me2 spreading into EIs (SI Appendix, Fig S7A), that was observed for all replicates (SI Appendix,
277 Fig S7B).

278 To further strengthen our analysis, we applied diffReps (50) on each replicate individually to
279 confirm differential enrichment of H3K9me2 in EIs of *caa39* and wt (Dataset S4). This very stringent
280 and not very sensitive analysis (essentially due to the fact that H3K9me2 peaks were barely
281 detectable in wt and that H3K9me2 spreading does not appear to be sequence-specific) could still
282 reveal increased levels of H3K9me2 in some EIs of *caa39*, but not all (92.0% in replicate 2, 73.9% in
283 replicate 3, 27.4% in replicate 1; Dataset S3). The limited number of EIs identified this way in replicate
284 1 can be attributed to the fact that it was less deeply sequenced than replicates 2 and 3 (GSE103924).
285 Despite that, there was a large overlap between replicates: among EIs that showed increased levels
286 of H3K9me2 in *caa39*, only one was identified in replicate 1 but not in replicates 2 or 3, and 96.4%
287 (161/167) of the EIs identified in replicate 3 were also identified in replicate 2 (SI

288 Appendix, Fig S7C, Dataset S3). We then extracted the number of significantly (diffReps G-test, $P <$
289 0.01) up or down H3K9me2 peaks in *caa39* versus wt, in each individual replicate (Dataset S4, sheet
290 4). A similar percentage of significantly up or down H3K9me2 peaks was observed at the genome
291 scale by this method (Fig 4D), in agreement with the fact that the global level of H3K9me2 does not
292 seem to be significantly affected in *caa39*. In contrast, the proportion of peaks was significantly
293 shifted toward gains of H3K9me2 within EIs, particularly within EI genes and their 5' UTRs (Fig 4D,
294 Dataset S4), confirming the specific role of Topo VI in safeguarding EI genes from ectopic spreading of
295 H3K9me2.

296 Globally, these data show that Topo VI is required to prevent elevated H3K9me2 levels within
297 EIs, presumably by preserving sharp boundaries between these insulated elements to avoid
298 pervasive spreading of heterochromatin from flanking regions. We further documented such a
299 barrier-like function on a S-EI containing a single gene, *At1g41830*, by ChIP-qPCR analysis of
300 H3K9me2. Scanning of six different loci along this region (Fig 4E) in independent experiments
301 confirmed the increased H3K9me2 levels within the island body, but also a decrease in one
302 neighboring heterochromatic border (Fig 4E), similarly to what was observed in the ChIP-seq
303 experiment replicates for this EIs (Fig 4I and SI Appendix, Fig S8) and other inspected EIs (SI Appendix,
304 Fig S8).

305

306 **EI gene repression is correlated with H3K9me2 spreading**

307 We then tried to evaluate the relative contribution of H3K9me2 increase to the
308 downregulation of EI genes, compared to other heterochromatin and repressive marks. Firstly,
309 because H3K9me2 and non-CG (CHG and CHH) DNA methylation are strongly inter-dependent (51),
310 we tested whether H3K9me2 spreading into EIs might in turn, or reciprocally, affect DNA
311 methylation. Whole-genome bisulfite sequencing revealed that DNA methylation levels in all
312 sequence contexts were overall unaltered in *caa39* relative to wt in EIs (Fig 4F and I, SI Appendix, Fig
313 S8). Differentially methylated region (DMR) analyses confirmed that there was no global significant
314 increase of DNA methylation in EIs (Dataset S5). Surprisingly, despite CHGs being known to be
315 methylated through a feedback loop with H3K9me2, DMR analyses rather revealed a very slight
316 decrease of CHG, with 51 hypo-CHG DMRs and 16 hyper-CHG DMRs observed in EIs of *caa39* (with
317 differences in the methylation percentage higher than 10%, $P < 0.05$, Dataset S5). Therefore, DNA
318 methylation does not seem to contribute to the downregulation of gene expression in EIs.

319 Secondly, because EI boundaries are enriched in H3K27me3-marked heterochromatin state
320 8, and that H3K27me3 is also found on the proximal promoter (chromatin state 2) and transcribed

321 region of many euchromatic genes (chromatin state 5, silenced genes) (49), we also performed a
322 genome-wide H3K27me3 analysis by CHIP-seq. Interestingly, we observed a globally inverted
323 tendency as compared to H3K9me2 profiles: average H3K27me3 levels were locally and significantly
324 decreased within EIs (SI Appendix, Fig S9A-B). We further documented such a local decrease of
325 H3K27me3 on the S-EI containing *At1g41830*, by CHIP-qPCR (SI Appendix, Fig S9C). Consistent with
326 this, K-means linear clustering revealed that H3K27me3 decrease could not be generalized to all EIs,
327 as it marks only a small subset of EIs in wt (Fig 4G). Thus, H3K27me3 does not seem to contribute to
328 the global downregulation of EI genes, and its local decrease at some EI genes might even
329 counterbalance the effect of H3K9me2 increase in a few EIs.

330 Finally, we directly compared EI gene expression with H3K9me2 changes. A vast majority
331 (90%) of EI genes that show significant changes ($P < 0.05$) in either RNA-seq or CHIP-seq analyses are
332 repressed and possess enhanced levels of H3K9me2 (Fig 4H and I, SI Appendix, Fig S8 and S10A).
333 Interestingly, the most repressed genes also tend to have the sharpest H3K9me2 increase, which is
334 particularly true in S-EIs. (Fig 4H, SI Appendix, Fig S10A). To see whether H3K9me2 defect might
335 affect the expression of EI genes, we generated the quadruple mutant *caa39 suvh456* mutated for
336 the H3K9 methylase genes *KRYPTONITE (KYP)/ SUVH4, SUVH5* and *SUVH6* and examined the
337 expression of the seven pericentromeric genes already studied. The expression of some EI genes was
338 significantly increased in *caa39 suvh456* as compared to *caa39* (Fig S10B). Taken together, these
339 results suggest that H3K9me2 increase plays a role in the reduced expression of EI genes, although
340 higher order chromatin structure, changes in other histone modification, and other indirect effects of
341 the *caa39* mutation may contribute to gene expression changes.

342

343 **The Topo VI subunit BIN4 physically associates with MAT3**

344 To gain knowledge on the molecular mechanism by which Topo VI contributes to the
345 delimitation of chromatin boundaries, we used the BIN4 subunit as a bait to screen a yeast two
346 hybrid (Y2H) cDNA library (Hybrigenics). A strong interaction with the Topo VI subunit RHL1 was
347 detected, thereby demonstrating the reliability of the screening procedure (Dataset S6). Among the
348 eleven additional interacting partners, three proteins belong to the S-AdenosylMethionine (SAM)
349 biosynthesis pathway, the universal methyl group donor (52). The first one, 5-methylthioribose-1-
350 phosphate isomerase (MTI1, AT2G05830), is involved in the methionine salvage pathway whereas
351 the two others, Methionine Synthase 1 (MS1, AT5G17920) and Methionine Adenosyltransferase 3
352 (MAT3, AT2G36880) are the ultimate enzymes of the SAM cycle. In order to identify BIN4-interacting
353 proteins *in planta*, we also performed a CoIP-MS experiment using the *Arabidopsis mid-1*

354 *35S:BIN4/MID-YFP* line, which consists of the *mid-1* allelic mutant of *BIN4* complemented with YFP-
355 tagged BIN4/MID (39), and a wt line as control. To exclude nonspecific proteins, we discarded
356 proteins that were not detected in both BIN4/MID-YFP CoIP-MS replicates, as well as plastidial,
357 mitochondrial and peroxisomal proteins. The presence of the RHL1 and TOP6B Topo VI subunits in
358 BIN4/MID-YFP CoIPs validated our procedure (Dataset S7). Remarkably, MAT3 co-
359 immunoprecipitated strongly with BIN4. MAT4 also co-immunoprecipitated with BIN4, but
360 apparently to a much lesser extent (Dataset S7). We further investigated the genetic and biochemical
361 interactions between BIN4 and enzymes of the SAM cycle, particularly the very last enzyme MAT3,
362 using Bimolecular Fluorescence Complementation (BiFC). We confirmed the BIN4-MAT3 and BIN4-
363 MS1 interactions in nuclei of transiently agro-transformed *Nicotiana benthamiana* mesophyll cells
364 (Fig 5A).

365

366 **MAT3 is required for H3K9me2**

367 Given that MAT enzymes synthesize the SAM required for DNA and histone methylation, and
368 that Topo VI is required for proper distribution of H3K9me2 throughout EI-containing
369 heterochromatic regions, we hypothesized that disruption of MAT3 affects H3K9me2 deposition. To
370 address this question, we used a recently characterized knock-down line in which *MAT3* 3'-UTR is
371 interrupted by a T-DNA (53), generating strongly reduced but still detectable transcripts levels (SI
372 Appendix, Fig S11A). We measured H3K9me2 levels at the four TEs strongly de-repressed in Topo VI
373 mutant plants (Fig 2) by ChIP-qPCR and found decreased levels of H3K9me2 (Fig 5B). This modest
374 decrease of H3K9me2 might be explained by the hypomorphic nature of the mutation or by a
375 functional redundancy between MAT isoforms that share over 85% amino acid sequence identity (SI
376 Appendix, Fig S11B). To test this hypothesis, we took advantage of a homozygous, mono-insertional,
377 co-suppressor transgenic line obtained during the process of generating *MAT3-YFP* overexpressors,
378 that we referred to as *MAT* KD (Fig 5C, SI Appendix, Fig S11C). Owing to their high DNA sequence
379 identity (SI Appendix, Fig S11D), all *MAT* genes are downregulated in this line (SI Appendix, Fig S11E).
380 In addition, the stochastic silencing of *MATs* gives rise to different phenotype severities: mildly
381 affected *MAT* KD plants (Fig 5C) that accumulate less *MATs* transcripts than wt (SI Appendix, Fig
382 S11E) and present a more severe phenotype than *mat3* hypomorphic mutant plants (Fig 5C); and
383 strongly affected *MAT* KD+ sister plants (Fig 5C) that accumulate even less *MAT* transcripts (SI
384 Appendix, Fig S11E). As anticipated, the H3K9me2 decrease was even more pronounced in *MAT* KD
385 plants than in *mat3* (Fig 5B). These results suggest that MAT isoforms possibly have additive roles in
386 H3K9 dimethylation. Given the decrease of H3K9me2 in MAT-deficient plants, we then determined

387 the extent of TE reactivation in *mat3* and *MAT* KD by RT-qPCR analysis of the same four TEs. We
388 observed increased levels of TE transcripts in *mat3* (Fig 5D). This increase was generally more
389 pronounced in *MAT* KD plants, particularly in *MAT* KD+ plants (Fig 5D). In contrast, we did not
390 observe any significant effect on EI gene expression (SI Appendix, Fig S11F).

391

392 **Topo VI favors MAT enrichment at some heterochromatin borders and depletion from euchromatic** 393 **islands**

394 Collectively, our results suggest that Topo VI and MAT3 could act together in maintaining
395 sharp chromatin boundaries by influencing H3K9me2 deposition. We therefore used a newly
396 developed anti-MAT antibody (Agrisera, Vännäs, Sweden) to test for MAT enrichment at specific loci
397 and a putative Topo VI dependency. First, the specificity of this antibody was validated by
398 immunoblot analysis of protein extracts from wt, *MAT* KD and *MAT3-YFP* overexpressing lines (SI
399 Appendix, Fig S12A). We then performed ChIP-qPCR using an anti-MAT antibody and chromatin from
400 wt and *caa39* plants, to measure the recovery of TEs that are reactivated upon Topo VI or MATs loss
401 of functions. Interestingly, MATs were enriched on all the tested TEs in wt and less in *caa39*, as
402 compared to an IgG negative control (Fig 6A). To specifically evaluate the implication of the BIN4/
403 MID-associated MAT3 isoform, we performed ChIP-qPCR using an anti-GFP antibody and chromatin
404 from two independent *MAT3-YFP* expressing lines. TEs reactivated in *MAT* KD and in Topo VI mutant
405 plants were also specifically enriched in the GFP-pulled down chromatin (SI Appendix, Fig S12B).
406 These results indicate that Topo VI is required for the association of MAT3 with heterochromatic
407 elements.

408 To test whether Topo VI might also influence the enrichment of MATs at EIs, we performed
409 ChIP-qPCR using an anti-MAT antibody and chromatin from wt and *caa39*, and analyzed the same EI
410 as in Figures 4E and I, which shows increased H3K9me2 levels within the island body (probe 3-4) but
411 decreased levels in the 5' heterochromatic border (probe 1) in *caa39* (Fig 4E and I, Fig 6B, top panel).
412 We detected a significant decrease of MAT occupancy in this border in *caa39* (Fig 6B, bottom panel,
413 probe 1) and, conversely, significantly enhanced MAT occupancy in the island body (probe 3) in
414 *caa39* compared to wt (Fig 6B, bottom panel, probes 3-4). We analyzed three other S-EIs that show
415 decreased gene expression levels (Fig 3C), increased internal H3K9me2 levels (Figs 4C and SI
416 Appendix, Fig S8) and contain a single gene (*At4g06634*'s and *At5g30495*'s EIs) or two genes
417 (*At2g07340*'s EIs). We observed trends of decreased MAT occupancy at one or both borders and
418 enhanced MAT occupancy in the island bodies of *caa39* (Fig 6C-E). These results suggest that the loss

419 of Topo VI leads to MAT redistribution over EIs, which correlates with H3K9me2 redistribution and
420 EIs heterochromatinization in *caa39*.

421 Discussion

422 The *Arabidopsis* epigenome is largely indexed by discrete chromatin signatures usually
423 corresponding to single genetic element (e.g., a gene or a TE) (49, 54). However, despite this, in
424 *Arabidopsis* DNA methylation has a known tendency to spread away from many TEs (55), and a few
425 other studies have reported the existence of heterochromatin spreading in plants (56–58). Yet, the
426 mechanisms that repress heterochromatin spreading, hence safeguarding EIs, are poorly understood
427 in plants. Our study confirmed the existence of an insulator-like mechanism that preserves EIs and
428 unveiled the role played by the Topo VI complex in this process. We first provide evidence that Topo
429 VI is required to preserve the euchromatic nature and transcriptional activity of gene islands within
430 pericentromeric and chromosome 4 knob heterochromatic regions. Indeed, the most remarkable
431 effect of the *caa39* mutation was the specific misregulation of pericentromeric elements, with a
432 general downregulation of EI genes and, inversely, a reactivation of some heterochromatic TEs. We
433 confirmed this peculiar expression pattern in several amorphic and hypomorphic mutants of the
434 Topo VI complex. Surprisingly, EI gene downregulation is more pronounced in the hypomorphic
435 mutants *caa39* and *BIN4* KD than in the corresponding null Topo VI mutants that display more severe
436 growth defects. Taking advantage of uncoupled growth defects and gene expression changes in the
437 hypomorphic *caa39* allele, we were able to show that the repression of EI genes is correlated with
438 the invasion of EIs by H3K9me₂, indicating that Topo VI is required to prevent the spreading of
439 H3K9me₂, here referred to as a boundary function. The increased expression of some EI genes in the
440 quadruple mutant *caa39 suvh456*, defective for the H3K9 methylase SUVH4, SUVH5 and SUVH6, as
441 compared with *caa39*, further supported that H3K9me₂ spreading over EI genes participates to some
442 extent in the transcriptional silencing of EI genes in Topo VI defective plants.

443 Although it is known that CHG methylation is maintained through a feedback loop with
444 H3K9me₂, WGBS identified no global increase of cytosine methylation over EIs in *caa39*, but rather a
445 slight decrease of CHG methylation, suggesting that DNA methylation is not involved in the reduced
446 expression of EI genes in Topo VI mutants. Other recent work has also shown that, under specific
447 circumstances, increased H3K9me₂ levels do not necessarily result in increased CHG or CHH
448 methylation, and vice versa. For instance, the AT-hook protein AHL10 ectopically recruits H3K9me₂
449 to small, AT-rich TEs without coincidental increase in DNA methylation (59). Conversely, the
450 expression of *AtCMT3* in *Eutrema Salsugineum*, a Brassicaceae that has lost *CMT3* and gene body
451 methylation, induces *de novo* gene body methylation in CHG, CHH and CG contexts, but without
452 resulting in stable gain of H3K9me₂. Interestingly, CHG hypermethylation in gene bodies is also not
453 correlated with consistent changes in gene expression in this case (60). While DNA methylation does
454 not appear to be involved in the reduced expression of EI genes in Topo VI mutants, the question of

455 the relative importance of H3K9me2 remains. Indeed, and firstly, the level of H3K9me2 in EIs of
456 *caa39* is still significantly lower than in canonical heterochromatin. This might result from histone H3
457 demethylation, a process that is likely still active in *caa39*. Alternatively, gain of H3K9me2 could be
458 the outcome of a subset of cells in which *caa39* mutation has a strong effect on H3K9me2
459 boundaries. Secondly, the negative correlation between EI gene expressions and H3K9me2 changes is
460 good, particularly in small EIs, but not very high, suggesting that H3K9me2 spreading over EI genes
461 cannot entirely explain the transcriptional silencing of EI genes. H3K9me2 spreading on EIs might, in
462 turn, affect the establishment of other chromatin modifications. For instance, in the *ibm1* mutant,
463 increased levels of H3K9me2 on gene bodies are associated with decreased levels of H3K4me1 and
464 transcriptional silencing (61). Conversely, in the *svh456* triple mutant, many TEs show a drastic
465 increase in H3K4me1 level, which is associated with transcriptional derepression and loss of
466 H3K9me2 (61). Therefore, it is plausible that other histone methylation changes also occur in *caa39*,
467 as we did observe for H3K27me3, which shows an opposite trend to H3K9me2 in EIs. Thus, H3K9me2
468 spreading might itself perturb H3K27me3 deposition by PRC2 and/or erasing by trithorax group (trxG)
469 proteins. This second hypothesis is supported by similar observations made in other organisms,
470 where the loss of Swi6/HP1 leads to H3K9me2 spreading across natural constitutive heterochromatin
471 boundaries in fission yeast (62), and alters H3K27me3 deposition on facultative heterochromatin in
472 *Neurospora crassa* (63).

473 In animals, insulator proteins like CTCF can participate in several distinct processes, e.g.
474 locally as a chromatin barrier and more globally on the formation of topologically associating
475 domains (64). Similarly, the disorganization of chromocenters and the partial loss of pericentromeric
476 TE silencing observed in Topo VI mutants might result from the loss of a local boundary function and,
477 possibly, also by the loss of a distinct, more global, architectural function of Topo VI in
478 heterochromatin condensation. Indeed, given that no obvious loss of DNA methylation and only a
479 partial decrease of H3K9me2 over TEs were observed in Topo VI mutant plants, the reactivation of
480 TEs is unlikely to be solely explained by decreased levels of these marks, but rather by a combined
481 loosening of their heterochromatic nature and of their higher order organization. Although causal link
482 between chromatin reorganization and TEs reactivation in plants is very disputed, a few recent
483 studies link chromatin organizers with TE derepression independently of DNA demethylation. For
484 instance, the natural depletion of histone 1 in sex cells is responsible of the reactivation of approx.
485 100 heterochromatic TEs via DNA demethylation-dependent (77/98) and -independent (21/98)
486 mechanisms (65). In addition, MORC proteins, which belong to the GHKL ATPases superfamily like
487 Topo VI, are required for the silencing of approx. 20 TEs and the formation of chromocenters without
488 impacting H3K9me2 and DNA methylation levels (66–68). Interestingly human CTCF has been shown

489 to interact with Topo II β (69, 70) and appears to be part of a protein interaction network that also
490 contains MORC2 and members of the cohesin complex in HeLa cells (71). Intriguingly, plant and
491 human recombinant MORC proteins seem to display a type II topoisomerase-like activity, which
492 requires additional plant extracts for full activity (72).

493 Given the function of MAT enzymes in the synthesis of SAM, MAT perturbation is expected to
494 affect a wide range of methylation reactions, which include DNA and histone methylations. The *mat3*
495 mutant line used in our study has been shown, however, to have global SAM levels similar to wt and
496 only very slightly reduced global levels of DNA methylations, unlike other *mat* mutants that show
497 more severe DNA and histone methylation defects (73). This suggests that the increased levels of
498 some TE transcripts in *mat3*, and the corresponding decreased levels of H3K9me₂, are more likely
499 attributable to a local effect of the *mat3* mutation, rather than a global decrease of SAM, or be the
500 outcome of a subset of cells in which *mat3* mutation has a strong effect. Our finding that the Topo VI
501 BIN4 subunit directly interacts with MAT3 and is required for MAT3 enrichment at some TE loci and
502 depletion from euchromatic islands, might provide a mechanistic explanation for such a local role of
503 MAT3 on chromatin, in addition to its general role in SAM synthesis (73). Similarly, the mammal
504 MATII α isoform also directly supplies SAM in the close vicinity of oncogenes to allow transcriptional
505 repression and H3K9me₂ deposition (74, 75). Intriguingly, the mouse MATII α has been found to
506 interact with Topoisomerase II α , a type IIA topoisomerase whose C-terminal regulatory domain
507 possesses sequence similarity with the BIN4 subunit of the plant Topo VI complex (38). Hence,
508 although this requires testing in other organisms, an interaction between MAT enzymes and type II
509 topoisomerases might be evolutionary conserved. Targeting of MATs to specific chromatin regions by
510 topoisomerases might be a way to couple SAM synthesis and availability *in situ*, possibly for DNA or
511 histone methylation. Extensive genome-wide studies will provide a general view of chromatin
512 modification changes in different *mat* mutants and their relative impacts on TE and gene expression.

513 In plants, the existence of an insulator-like function that would partition chromatin into
514 different functional domains has long been questioned (9, 11, 26). We show that Topo VI participates
515 to such a function by preventing the spreading of the heterochromatic mark H3K9me₂ into
516 neighboring euchromatin islands. Our results suggest that the prevention of heterochromatin
517 spreading might rely upon a Topo VI-MAT3 interaction that would be important for the proper
518 targeting of MAT3 to heterochromatin and its exclusion from euchromatic islands. Future studies
519 might allow the identification of direct molecular links between Topo VI, MAT proteins and
520 methyltransferases involved in DNA and histone methylation, for fine-tuning the establishment of
521 sharp transitions in chromatin identity along the genome.

522 **Materials and Methods**

523 Detailed descriptions of the experimental methods are provided in SI Appendix, Supplementary
524 Materials and Methods. These include cloning procedures, plant material and growth conditions,
525 DNA preparation, Chop- and ChIP-qPCR, anti-5-meC ELISA assay, yeast two-hybrid screen, co-
526 immunoprecipitation-MS, Western blot, RNA extraction, RT-qPCR and microarrays, RNA-seq library
527 preparation and sequencing, RNA-seq bioinformatic treatment and analysis, whole-genome bisulfite
528 sequencing and DNA methylation analysis, chromatin immunoprecipitation, ChIP-seq analysis,
529 immunofluorescence, transient transformation and protoplasts preparation, confocal and
530 epifluorescence microscopy.

531

532 **Availability of data and material**

533 ChIP-seq, RNA-seq, BS-seq and microarray datasets are available at
534 <https://www.ncbi.nlm.nih.gov/geo/query/acc.cgi?acc=GSE103924> (reviewer token:
535 slchuqakvwwfpsi). Custom scripts used in this study are available at [https://github.com/michel-](https://github.com/michel-teresse)
536 [teresse](https://github.com/michel-teresse).

537

538 **Acknowledgments**

539 We thank Imen Mestiri (IBENS, Paris) for her expertise with cytogenetics. We also want to express
540 our gratitude to students who contributed to this work, especially Justine Quillet, Julien Vieu and
541 César Botella. We thank Ben Field for critical reading of the manuscript. This work was supported by
542 the French National Research Agency (ANR 2010-JCJC-1205-01 and ANR-14-CE02-0010 to CL). Work
543 by FB was supported by the Investissements d’Avenir LabexMemory in Living Systems (MEMOLIFE)
544 grant ANR-10-LABX-54. LD was supported by CEA and Région PACA. High-throughput RNA-
545 sequencing was performed at the POPS platform, supported by the LabEx Saclay Plant Sciences-SPS
546 (ANR-10-LABX-0040-SPS). MS analysis was performed at the IMM platform supported by a grant
547 from GIS IBiSA. High-throughput ChIP-seq was performed at the TGML platform, supported by grants
548 from Inserm, GIS IBiSA, Aix-Marseille Université, and ANR-10-INBS-0009-10.

549

550 **Author contributions**

551 LVM, FV, CV, LD, MR, and CB performed the experiments. CL and MT performed the bioinformatic
552 analyses. LST was in charge of the sequencing. LVM, CL, FB and CL analyzed the data. LVM, KS, FB and
553 CL designed the research. LVM, FB and CL wrote the manuscript. All authors read and approved the
554 final manuscript.

555

556 **Conflict of interest**

557 The authors declare that they have no conflict of interest

558

559

560 **References**

- 561 1. J. Wang, S. T. Lawry, A. L. Cohen, S. Jia, Chromosome boundary elements and regulation of
562 heterochromatin spreading. *Cell. Mol. Life Sci.* **71**, 4841–4852 (2014).
- 563 2. H. J. Muller, Types of visible variations induced by X-rays in *Drosophila*. *J. Genet.* **22**, 299–334
564 (1930).
- 565 3. T. Ali, R. Renkawitz, M. Bartkuhn, Insulators and domains of gene expression. *Curr. Opin.*
566 *Genet. Dev.* **37**, 17–26 (2016).
- 567 4. W. A. Bickmore, B. van Steensel, Genome Architecture: Domain Organization of Interphase
568 Chromosomes. *Cell* **152**, 1270–1284 (2013).
- 569 5. J. Dekker, T. Misteli, Long-Range Chromatin Interactions. *Cold Spring Harb. Perspect. Biol.* **7**,
570 a019356 (2015).
- 571 6. J. R. Dixon, *et al.*, Topological domains in mammalian genomes identified by analysis of
572 chromatin interactions. *Nature* **485**, 376–380 (2012).
- 573 7. B. Bonev, G. Cavalli, Organization and function of the 3D genome. *Nat. Rev. Genet.* **17**, 772–
574 772 (2016).
- 575 8. P. Heger, B. Marin, M. Bartkuhn, E. Schierenberg, T. Wiehe, The chromatin insulator CTCF and
576 the emergence of metazoan diversity. *Proc. Natl. Acad. Sci.* **109**, 17507–17512 (2012).
- 577 9. C. Wang, *et al.*, Genome-wide analysis of local chromatin packing in *Arabidopsis thaliana*.
578 *Genome Res.* **25**, 246–256 (2015).

- 579 10. S. D. Singer, J. M. Hily, K. D. Cox, Analysis of the enhancer-blocking function of the TBS
580 element from *Petunia hybrida* in transgenic *Arabidopsis thaliana* and *Nicotiana tabacum*.
581 *Plant Cell Rep.* **30**, 2013–2025 (2011).
- 582 11. C. Liu, Y.-J. Cheng, J.-W. Wang, D. Weigel, Prominent topologically associated domains
583 differentiate global chromatin packing in rice from *Arabidopsis*. *Nat. Plants* **3**, 742–748 (2017).
- 584 12. C. Liu, D. Weigel, Chromatin in 3D: progress and prospects for plants. *Genome Biol.* **16**, 170
585 (2015).
- 586 13. J. Sequeira-Mendes, C. Gutierrez, Genome architecture: from linear organisation of chromatin
587 to the 3D assembly in the nucleus. *Chromosoma* **125**, 455–469 (2016).
- 588 14. S. Grob, M. W. Schmid, N. W. Luedtke, T. Wicker, U. Grossniklaus, Characterization of
589 chromosomal architecture in *Arabidopsis* by chromosome conformation capture. *Genome*
590 *Biol.* **14**, R129 (2013).
- 591 15. S. Grob, M. W. Schmid, U. Grossniklaus, Hi-C Analysis in *Arabidopsis* Identifies the KNOT , a
592 Structure with Similarities to the flamenco Locus of *Drosophila*. *Mol. Cell* **55**, 678–693 (2014).
- 593 16. S. Feng, *et al.*, Genome-wide Hi-C Analyses in Wild-Type and Mutants Reveal High-Resolution
594 Chromatin Interactions in *Arabidopsis*. *Mol. Cell* **55**, 694–707 (2014).
- 595 17. A. Veluchamy, *et al.*, LHP1 Regulates H3K27me3 Spreading and Shapes the Three-Dimensional
596 Conformation of the *Arabidopsis* Genome. *PLoS One* **11**, e0158936 (2016).
- 597 18. C. Liu, *et al.*, Genome-wide analysis of chromatin packing in *Arabidopsis thaliana* at single-
598 gene resolution. *Genome Res.* **26**, 1057–1068 (2016).
- 599 19. P. Fransz, H. De Jong, From nucleosome to chromosome: A dynamic organization of genetic
600 information. *Plant J.* **66**, 4–17 (2011).
- 601 20. L. Simon, M. Voisin, C. Tatout, A. V. Probst, Structure and function of centromeric and
602 pericentromeric heterochromatin in *Arabidopsis thaliana*. *Front. Plant Sci.* **6**, 1–8 (2015).
- 603 21. S. Del Prete, J. Arpón, K. Sakai, P. Andrey, V. Gaudin, Nuclear Architecture and Chromatin
604 Dynamics in Interphase Nuclei of *Arabidopsis thaliana*. *Cytogenet. Genome Res.* **143**, 28–50
605 (2014).
- 606 22. P. Fransz, J. H. de Jong, M. Lysak, M. R. Castiglione, I. Schubert, Interphase chromosomes in
607 *Arabidopsis* are organized as well defined chromocenters from which euchromatin loops
608 emanate. *Proc. Natl. Acad. Sci.* **99**, 14584–14589 (2002).

- 609 23. W. J. J. Soppe, *et al.*, DNA methylation controls histone H3 lysine 9 methylation and
610 heterochromatin assembly in Arabidopsis. *EMBO J.* **21**, 6549–6559 (2002).
- 611 24. O. Mathieu, A. V Probst, J. Paszkowski, Distinct regulation of histone H3 methylation at lysines
612 27 and 9 by CpG methylation in Arabidopsis. *EMBO J.* **24**, 2783–2791 (2005).
- 613 25. Z. Lippman, *et al.*, Role of transposable elements in heterochromatin and epigenetic control.
614 *Nature* **430**, 471–476 (2004).
- 615 26. Z. Vergara, C. Gutierrez, Emerging roles of chromatin in the maintenance of genome
616 organization and function in plants. *Genome Biol.* **18**, 96 (2017).
- 617 27. A. Bergerat, D. Gabelle, P. Forterre, Purification of a DNA topoisomerase II from the
618 hyperthermophilic archaeon *Sulfolobus shibatae*. A thermostable enzyme with both bacterial
619 and eucaryal features. *J. Biol. Chem.* **269**, 27663–27669 (1994).
- 620 28. A. Bergerat, *et al.*, An atypical topoisomerase II from archaea with implications for meiotic
621 recombination. *Nature* **386**, 414–417 (1997).
- 622 29. K. Schneider, *et al.*, The ROOT HAIRLESS 1 gene encodes a nuclear protein required for root
623 hair initiation in Arabidopsis. *Genes (Basel)*. **12**, 2013–2021 (1998).
- 624 30. K. Schneider, B. Wells, L. Dolan, K. Roberts, Structural and genetic analysis of epidermal cell
625 differentiation in Arabidopsis primary roots. *Development* **124**, 1789–1798 (1997).
- 626 31. K. Sugimoto-Shirasu, *et al.*, RHL1 is an essential component of the plant DNA topoisomerase
627 VI complex and is required for ploidy-dependent cell growth. *Proc. Natl. Acad. Sci. U. S. A.*
628 **102**, 18736–41 (2005).
- 629 32. H. J. Yoon, *et al.*, Lotus japonicus SUNERGOS1 encodes a predicted subunit A of a DNA
630 topoisomerase VI that is required for nodule differentiation and accommodation of rhizobial
631 infection. *Plant J.* **78**, 811–821 (2014).
- 632 33. F. Hartung, H. Puchta, Molecular characterization of homologues of both subunits A (SPO11)
633 and B of the archaeobacterial topoisomerase 6 in plants. *Gene* **271**, 81–86 (2001).
- 634 34. F. Hartung, *et al.*, An archaeobacterial topoisomerase homolog not present in other eukaryotes
635 is indispensable for cell proliferation of plants. *Curr. Biol.* **12**, 1787–1791 (2002).
- 636 35. Y. Yin, *et al.*, A crucial role for the putative Arabidopsis topoisomerase VI in plant growth and
637 development. *Proc. Natl. Acad. Sci. U. S. A.* **99**, 10191–6 (2002).

- 638 36. A. Mittal, *et al.*, TOPOISOMERASE 6B is involved in chromatin remodelling associated with
639 control of carbon partitioning into secondary metabolites and cell walls, and epidermal
640 morphogenesis in Arabidopsis. *J. Exp. Bot.* **65**, 4217–4239 (2014).
- 641 37. K. Sugimoto-shirasu, N. J. Stacey, J. Corsar, K. Roberts, M. C. Mccann, DNA Topoisomerase VI
642 Is Essential for Endoreduplication in Arabidopsis. *Curr. Biol.* **12**, 1782–1786 (2002).
- 643 38. C. Breuer, *et al.*, BIN4, a Novel Component of the Plant DNA Topoisomerase VI Complex, Is
644 Required for Endoreduplication in Arabidopsis. *Plant Cell* **19**, 3655–3668 (2007).
- 645 39. V. Kirik, A. Schrader, J. F. Uhrig, M. Hulskamp, MIDGET unravels functions of the Arabidopsis
646 topoisomerase VI complex in DNA endoreduplication, chromatin condensation, and
647 transcriptional silencing. *Plant Cell* **19**, 3100–3110 (2007).
- 648 40. E. L. Meczes, K. L. Gilroy, K. L. West, C. a Austin, The Impact of the Human DNA
649 Topoisomerase II C-Terminal Domain on Activity. *PLoS One* **3**, e1754 (2008).
- 650 41. A. Onoda, *et al.*, Nuclear dynamics of topoisomerase II β reflects its catalytic activity that is
651 regulated by binding of RNA to the C-terminal domain. *Nucleic Acids Res.* **42**, 9005–9020
652 (2014).
- 653 42. K. L. Gilroy, C. A. Austin, The Impact of the C-Terminal Domain on the Interaction of Human
654 DNA Topoisomerase II α and β with DNA. *PLoS One* **6**, e14693 (2011).
- 655 43. Y. Pommier, Y. Sun, S.-Y. N. Huang, J. L. Nitiss, Roles of eukaryotic topoisomerases in
656 transcription, replication and genomic stability. *Nat. Rev. Mol. Cell Biol.* **17**, 703–721 (2016).
- 657 44. M. Jain, A. K. Tyagi, J. P. Khurana, Overexpression of putative topoisomerase 6 genes from rice
658 confers stress tolerance in transgenic Arabidopsis plants. *FEBS J.* **273**, 5245–5260 (2006).
- 659 45. M. Jain, A. K. Tyagi, J. P. Khurana, Constitutive expression of a meiotic recombination protein
660 gene homolog, OsTOP6A1, from rice confers abiotic stress tolerance in transgenic Arabidopsis
661 plants. *Plant Cell Rep.* **27**, 767–778 (2008).
- 662 46. K. Simkova, *et al.*, Integration of stress-related and reactive oxygen species-mediated signals
663 by Topoisomerase VI in Arabidopsis thaliana. *Proc. Natl. Acad. Sci.* **109**, 16360–16365 (2012).
- 664 47. C. J. Underwood, I. R. Henderson, R. A. Martienssen, Genetic and epigenetic variation of
665 transposable elements in Arabidopsis. *Curr. Opin. Plant Biol.* **36**, 135–141 (2017).
- 666 48. K. De Preter, R. Barriot, F. Speleman, J. Vandesompele, Y. Moreau, Positional gene enrichment
667 analysis of gene sets for high-resolution identification of overrepresented chromosomal

- 668 regions. *Nucleic Acids Res.* **36**, 1–6 (2008).
- 669 49. J. Sequeira-Mendes, *et al.*, The Functional Topography of the Arabidopsis Genome Is
670 Organized in a Reduced Number of Linear Motifs of Chromatin States. *Plant Cell* **26**, 2351–
671 2366 (2014).
- 672 50. L. Shen, *et al.*, diffReps: Detecting Differential Chromatin Modification Sites from ChIP-seq
673 Data with Biological Replicates. *PLoS One* **8**, e65598 (2013).
- 674 51. H. Stroud, *et al.*, Non-CG methylation patterns shape the epigenetic landscape in Arabidopsis.
675 *Nat. Struct. Mol. Biol.* **21**, 64–72 (2014).
- 676 52. P. Zhang, MetaCyc and AraCyc. Metabolic Pathway Databases for Plant Research. *Plant*
677 *Physiol.* **138**, 27–37 (2005).
- 678 53. Y. Chen, T. Zou, S. McCormick, S -Adenosylmethionine Synthetase 3 Is Important for Pollen
679 Tube Growth. *Plant Physiol.* **172**, 244–253 (2016).
- 680 54. F. Roudier, *et al.*, Integrative epigenomic mapping defines four main chromatin states in
681 Arabidopsis. *EMBO J.* **30**, 1928–1938 (2011).
- 682 55. I. Ahmed, A. Sarazin, C. Bowler, V. Colot, H. Quesneville, Genome-wide evidence for local DNA
683 methylation spreading from small RNA-targeted sequences in Arabidopsis. *Nucleic Acids Res.*
684 **39**, 6919–6931 (2011).
- 685 56. S. R. Eichten, *et al.*, Spreading of Heterochromatin Is Limited to Specific Families of Maize
686 Retrotransposons. *PLoS Genet.* **8**, e1003127 (2012).
- 687 57. Z. Lang, *et al.*, The Methyl-CpG-Binding Protein MBD7 Facilitates Active DNA Demethylation to
688 Limit DNA Hyper-Methylation and Transcriptional Gene Silencing. *Mol. Cell* **57**, 971–983
689 (2015).
- 690 58. H. Saze, A. Shiraishi, A. Miura, T. Kakutani, Control of Genic DNA Methylation by a jmjC
691 Domain-Containing Protein in Arabidopsis thaliana. *Science (80-.)*. **319**, 462–465 (2008).
- 692 59. H. Jiang, *et al.*, Ectopic application of the repressive histone modification H3K9me2
693 establishes post-zygotic reproductive isolation in Arabidopsis thaliana. *Genes Dev.* **31**, 1272–
694 1287 (2017).
- 695 60. J. M. Wendte, *et al.*, Epimutations are associated with CHROMOMETHYLASE 3-induced de
696 novo DNA methylation. *Elife* **8** (2019).

- 697 61. S. Inagaki, *et al.*, Gene-body chromatin modification dynamics mediate epigenome
698 differentiation in *Arabidopsis*. *EMBO J.* **36**, 970–980 (2017).
- 699 62. R. Stunnenberg, *et al.*, H3K9 methylation extends across natural boundaries of
700 heterochromatin in the absence of an HP1 protein. *EMBO J.* **34**, 2789–2803 (2015).
- 701 63. K. Jamieson, *et al.*, Loss of HP1 causes depletion of H3K27me3 from facultative
702 heterochromatin and gain of H3K27me2 at constitutive heterochromatin. *Genome Res.* **26**,
703 97–107 (2016).
- 704 64. Y. Lu, G. Shan, J. Xue, C. Chen, C. Zhang, Defining the multivalent functions of CTCF from
705 chromatin state and three-dimensional chromatin interactions. *Nucleic Acids Res.* **44**, 6200–
706 6212 (2016).
- 707 65. S. He, M. Vickers, J. Zhang, X. Feng, Natural depletion of histone H1 in sex cells causes DNA
708 demethylation, heterochromatin decondensation and transposon activation. *Elife* **8**, 1–23
709 (2019).
- 710 66. G. Moissiard, *et al.*, MORC family ATPases required for heterochromatin condensation and
711 gene silencing. *Science* **336**, 1448–51 (2012).
- 712 67. Z. J. Lorkovi, U. Naumann, A. J. M. Matzke, M. Matzke, Involvement of a GHKL ATPase in RNA-
713 Directed DNA Methylation in *Arabidopsis thaliana*. *Curr. Biol.* **22**, 933–938 (2012).
- 714 68. T. R. Brabbs, *et al.*, The stochastic silencing phenotype of *Arabidopsis morc6* mutants reveals a
715 role in efficient RNA -directed DNA methylation. *Plant J.* **75**, 836–846 (2013).
- 716 69. M. Witcher, B. M. Emerson, Epigenetic Silencing of the p16INK4a Tumor Suppressor Is
717 Associated with Loss of CTCF Binding and a Chromatin Boundary. *Mol. Cell* **34**, 271–284
718 (2009).
- 719 70. T. M. Yusufzai, H. Tagami, Y. Nakatani, G. Felsenfeld, CTCF Tethers an Insulator to Subnuclear
720 Sites, Suggesting Shared Insulator Mechanisms across Species. *Mol. Cell* **13**, 291–298 (2004).
- 721 71. L. Uusküla-reimand, *et al.*, Topoisomerase II beta interacts with cohesin and CTCF at
722 topological domain borders. *Genome Biol.* **17**, 1–22 (2016).
- 723 72. M. Manohar, *et al.*, Plant and human MORC proteins have DNA modifying activities similar to
724 type II topoisomerases, but require additional factor(s) for full activity. *Mol. Plant. Microbe.*
725 *Interact.* **30**, 87–100 (2017).
- 726 73. J. Meng, *et al.*, METHIONINE ADENOSYLTRANSFERASE4 Mediates DNA and Histone

- 727 Methylation. *Plant Physiol.* **177**, 652–670 (2018).
- 728 74. Y. Katoh, *et al.*, Methionine Adenosyltransferase II Serves as a Transcriptional Corepressor of
729 Maf Oncoprotein. *Mol. Cell* **41**, 554–566 (2011).
- 730 75. Y. Kera, *et al.*, Methionine Adenosyltransferase II-dependent Histone H3K9 Methylation at the
731 COX-2 Gene Locus. *J. Biol. Chem.* **288**, 13592–13601 (2013).
- 732 76. H. Thorvaldsdóttir, J. T. Robinson, J. P. Mesirov, Integrative Genomics Viewer (IGV): High-
733 performance genomics data visualization and exploration. *Brief. Bioinform.* **14**, 178–192
734 (2013).
- 735

736 **Figure legends**

737 **Figure 1. Topoisomerase VI is required for heterochromatin organization.** (A) Representative
738 nucleus ($n > 30$) from 6-day-old wt and *caa39* cotyledon epidermal cells stained with DAPI and
739 showing indirect immunolocalization of H3K9me2. Scale bar: 5 μ m. (B) Two independently prepared
740 nuclear extracts of wt and *caa39* were immunoblotted against H3 or H3K9me2, as indicated. (C)
741 Same as (A) for 5-meC localization. (D) Elisa assay to quantify total 5-meC in 6-day-old cotyledons of
742 wt, *caa39* and *ddm1-8*. **: $P < 0.005$ (Student's *t*-test).

743

744 **Figure 2. Topo VI is required for the silencing of transposable elements.** (A) Bar chart showing the
745 proportions of reactivated TE superfamilies in *caa39* compared to the general proportion of TEs in
746 the genome. The relative percentage is shown for each superfamily and the absolute number of
747 reactivated TEs is noted above each bar. **: $P < 0.005$; ****: $P < 0.0001$ (Chi-squared test). (B) RT-
748 qPCR confirmation of the reactivation of selected TEs in *caa39*, *rhl2-1* and *bin4-1*. Error bars: \pm SEM
749 of three biological replicates. *: $P < 0.05$; **: $P < 0.005$; ***: $P < 0.0005$ (Student's *t*-test). (C) DNA
750 from indicated genotypes were extracted and digested with McrBC. The mean ratio of digested over
751 undigested DNA from three biological replicates is shown. Error bars: \pm SEM of three biological
752 replicates. *: $P < 0.05$; **: $P < 0.005$; ***: $P < 0.0005$ (Student's *t*-test). (D) Average distribution of
753 methylated cytosine in CG, CHG and CHH contexts over TEs and 2 kb flanking regions. Two
754 independent replicates for each genotype were performed. (E) CHIP-qPCR of H3K9me2 at selected
755 TEs. Error bars: \pm SEM of three biological replicates. *: $P < 0.05$; **: $P < 0.005$; ***: $P < 0.0005$
756 (Student's *t*-test). (F) Average distribution of H3-normalized H3K9me2 over TEs and 2 kb flanking
757 regions. Two (H3) and three (H3K9me2) independent biological replicates for each genotype were
758 performed.

759

760 **Figure 3. Genes in euchromatic islands within heterochromatic pericentromeric and chromosome 4**
761 **knob regions are repressed in Topo VI mutants.** (A) Positional Gene Enrichment (PGE) analysis of the
762 top 500 most downregulated genes in *caa39*. The bed files corresponding to coordinates of the
763 widest enriched regions ($FDR < 0.05$) were visualized with a genome browser. Black lines correspond
764 to enriched regions, blue boxes correspond to pericentromeric regions as defined by Yelina et al.
765 (2012), green box to the knob and red to centromeres. (B) Scatter plots and Pearson correlations of
766 differentially expressed ($P < 0.05$) pericentromeric genes in *caa39* and *bin4-1* or *bin4-2*. (C) RT-qPCR
767 of selected pericentromeric genes in *caa39*, *rhl2-1*, *bin4-1* and *BIN4* KD at 6 days post-germination.
768 Error bars: \pm SEM of three biological replicates. **: $P < 0.005$; ***: $P < 0.0005$; ****: $P < 0.0001$ (two-

769 way ANOVA, Dunnett's test). (D) The proportion of each chromatin state was computed for EIs and
770 their 1.5 kb flanking regions. EI: Euchromatic Islands. (E) Gene content in EIs.

771

772 **Figure 4. Topo VI prevents the invasion of euchromatic islands by H3K9me2.** (A) ChIP-qPCR analysis
773 of H3K9me2 at EI genes. Error bars: \pm SEM of two biological replicates. *: $P < 0.05$; ***: $P < 0.0005$;
774 ****: $P < 0.0001$ (two-way ANOVA, Fisher's test). (B) Average distribution of H3-normalized
775 H3K9me2 along short euchromatic gene islands and 4 kb flanking regions. Two (H3) and three
776 (H3K9me2) independent biological replicates for each genotype were performed. P -value was
777 computed for each aggregated point by using the Mann-Whitney test. (C) Same as (B) long EIs. (D)
778 Bar chart showing the average percentage of down or up H3K9me2 peaks identified by diffReps
779 analysis in the genome, EIs, EI genes (EIGs), EI gene body, 5' and 3' UTRs. Error bars: \pm SEM of three
780 biological replicates. *: $P < 0.05$; ***: $P < 0.0005$; ****: $P < 0.0001$ (two-way ANOVA, Fisher's test). (E)
781 ChIP-qPCR validation of a single-gene island for H3K9me2. Error bars: \pm SEM of three biological
782 replicates. *: $P < 0.05$; ****: $P < 0.0001$ (two-way ANOVA, Fisher's test). (F) Average distribution of
783 methylated cytosine in CG, CHG and CHH contexts over EIs. Two independent replicates for each
784 genotype were performed. (G) K-means linear clustering of H3K9me2 and H3K27me3 tag densities
785 across EIs and their 900 nt flanking borders as revealed by seqMINER in *caa39* and wt. (H) Heatmap
786 correlation clustering of EI genes with significant changes in RNA-seq and H3K9me2/H3 ChIP-seq. (I)
787 Integrative Genomics Viewer (76) screenshot of H3, H3K9me2, H3K27me3, RNA, CG, CHG and CHH
788 methylation profiles in wt and *caa39* on a single gene-containing island. Each track is normalized
789 against corresponding input samples (ChIP-seq) and by the sequencing depth. Numbers indicate the
790 position of primers used in (E).

791

792 **Figure 5. MAT3 interacts with Topo VI and is required for H3K9me2 deposition on heterochromatic**
793 **loci.**

794 (A) Protoplasts from transiently agrotransformed *N. benthamiana* leaves expressing different
795 combination of BiFC vectors, as indicated. Nuclei were stained with Hoechst 33342. (B) Chromatin of
796 3 week-old wt or *MAT* KD (here a mixed pool of *MATs* silenced plants with strong or weak
797 phenotype) rosette leaves, or 6 day-old wt or *mat3* cotyledon nuclei was immunoprecipitated with
798 anti-H3K9me2 antibodies and the recovery of TEs known to be reactivated in *caa39* was assessed by
799 qPCR. The result is shown as a percentage of recovery normalized against wt. Error bars: \pm SEM of
800 two biological replicates. *: $P < 0.05$; **: $P < 0.005$; ***: $P < 0.0005$; ****: $P < 0.0001$ (two-way
801 ANOVA, Dunnett's test). (C) Representative photographs of 4-week-old wt, *MATs* silenced plants with

802 stronger (*MAT* KD+) and weaker (*MAT* KD) developmental phenotypes, and the *mat3* mutant. (D) RT-
803 qPCR analysis of TE transcript abundance in indicated genotypes. Error bars: \pm SEM of three biological
804 replicates. *: $P < 0.05$; **: $P < 0.005$; ***: $P < 0.0005$ (Student's *t*-test).

805

806 **Figure 6. Topo VI is required for MAT enrichment at heterochromatin borders and exclusion from**
807 **euchromatic islands.** (A) Chromatin of 6-day-old wt or *caa39* cotyledon nuclei was
808 immunoprecipitated with anti-MATs antibodies and the recovery of TEs reactivated in *MATs* silenced
809 plants and *caa39* was measured by qPCR. Error bars: \pm SEM of three biological replicates. (B-E) Top
810 panels: Integrative Genomics Viewer screenshots of H3- and sequencing depth-normalized H3K9me2
811 profiles, and locations of primers used in bottom panels. Bottom panels: Same as (A) on EIs
812 containing repressed genes in *caa39* such as *AT1G41830* (B), *AT4G06634* (C), *AT2G07340* (D) and
813 *AT5G30495* (E). Error bars: \pm SEM of two biological replicates. *: $P < 0.05$; **: $P < 0.005$; ***: $P <$
814 0.0005 (Student's *t*-test).

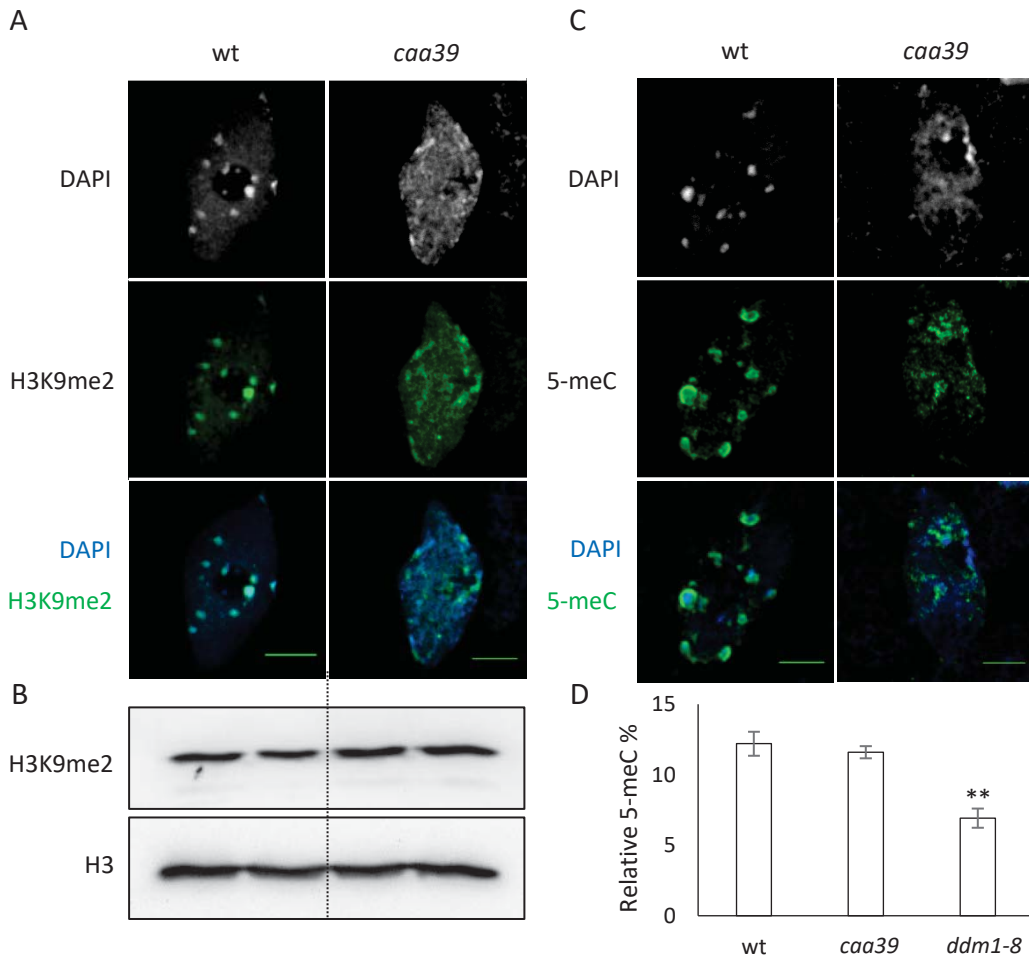


Fig 1

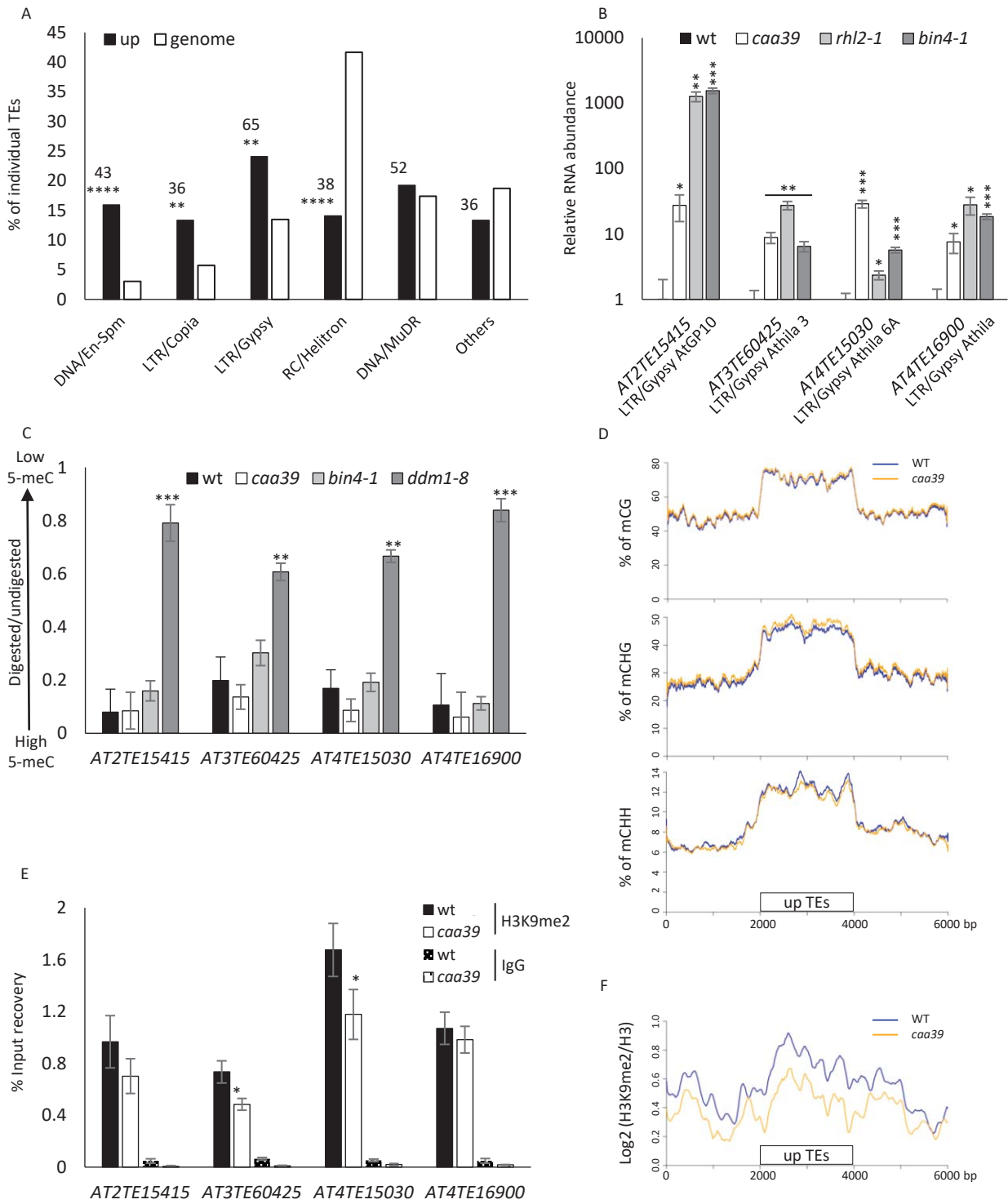


Fig 2

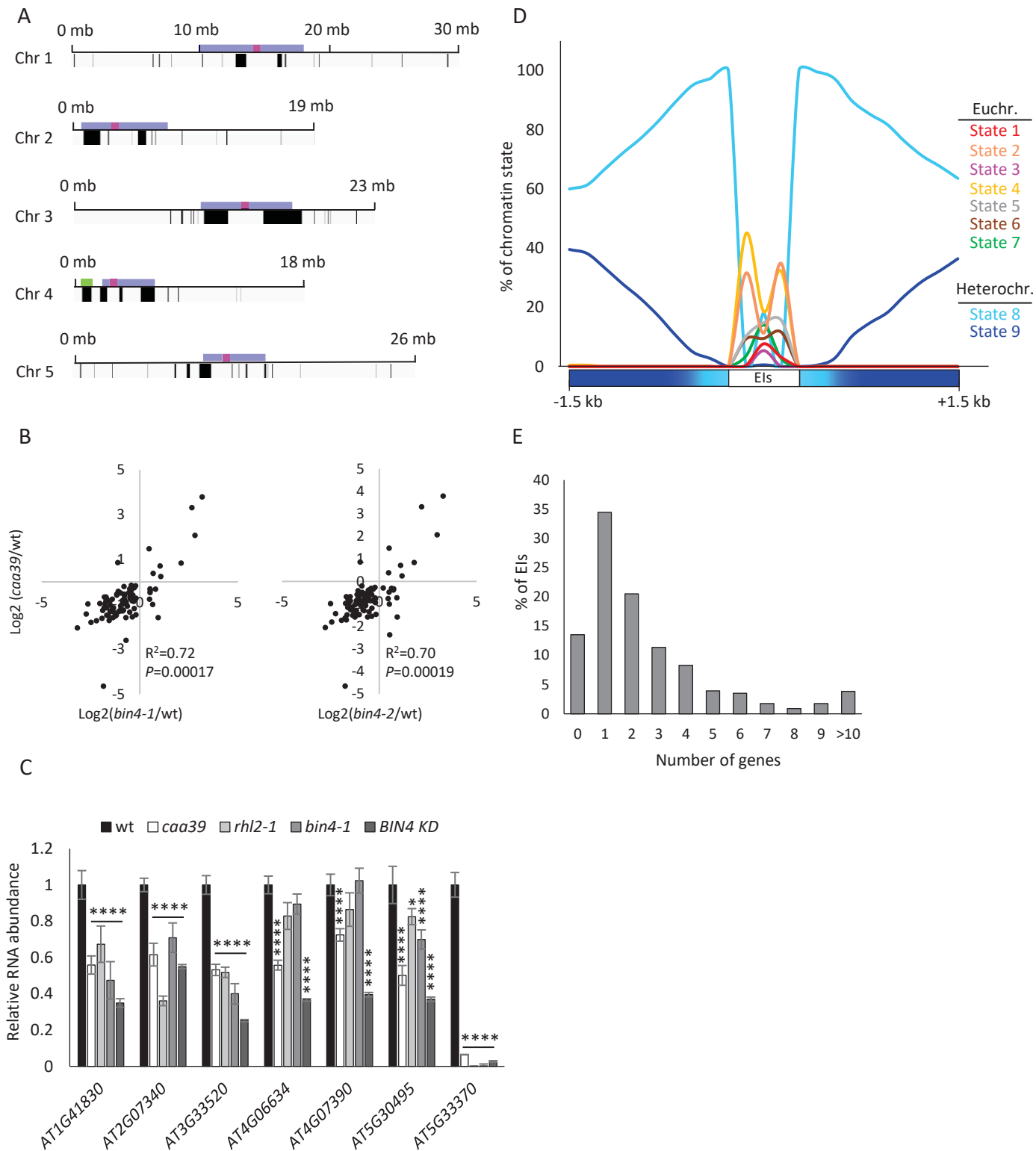


Fig 3

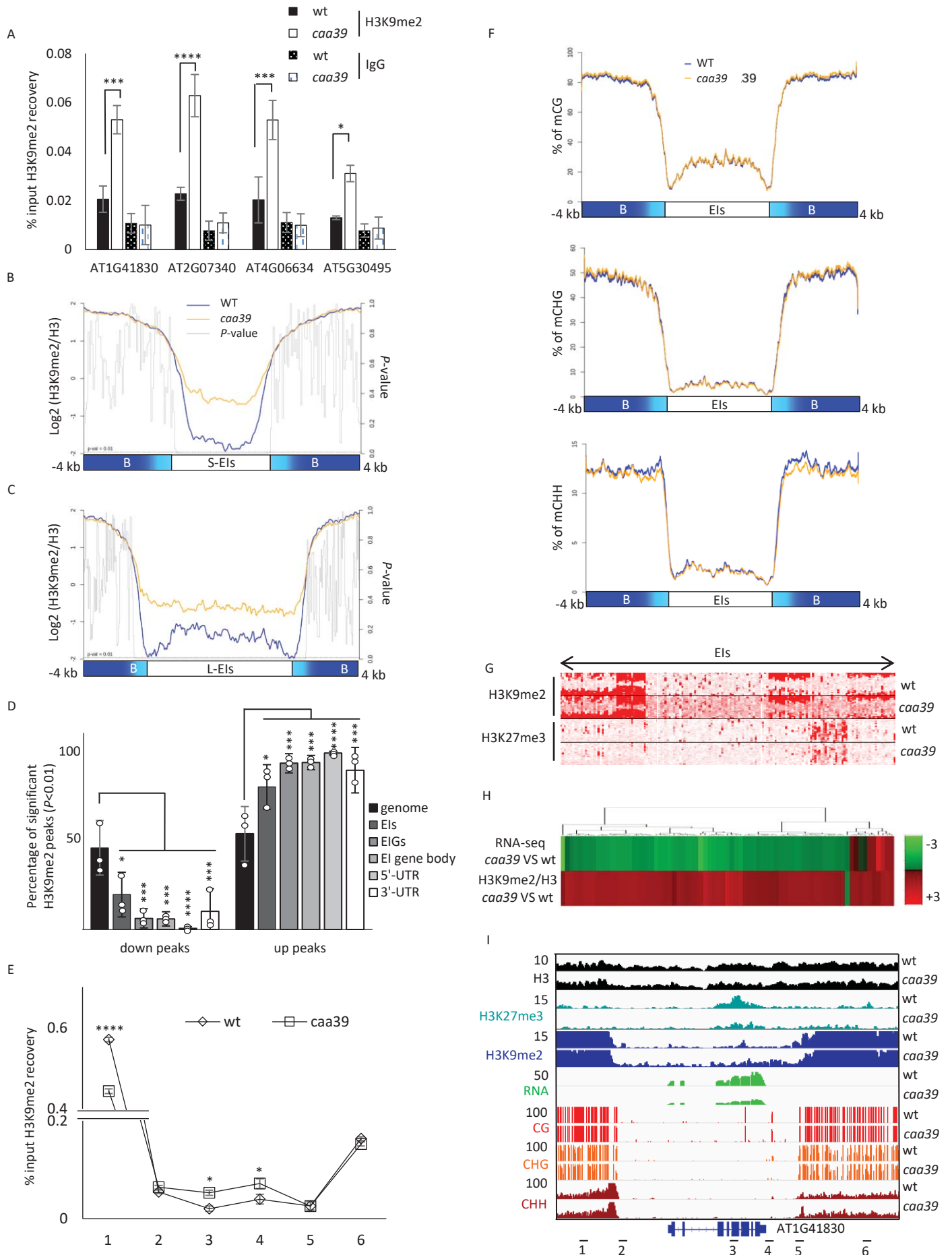


Fig 4

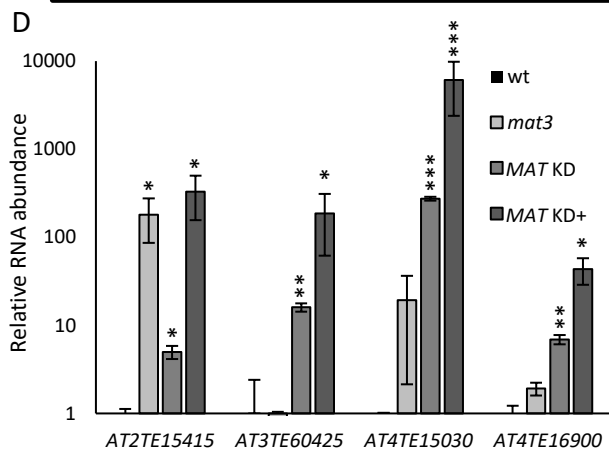
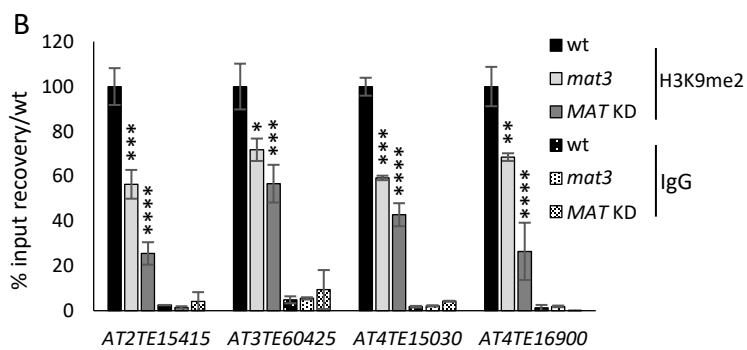
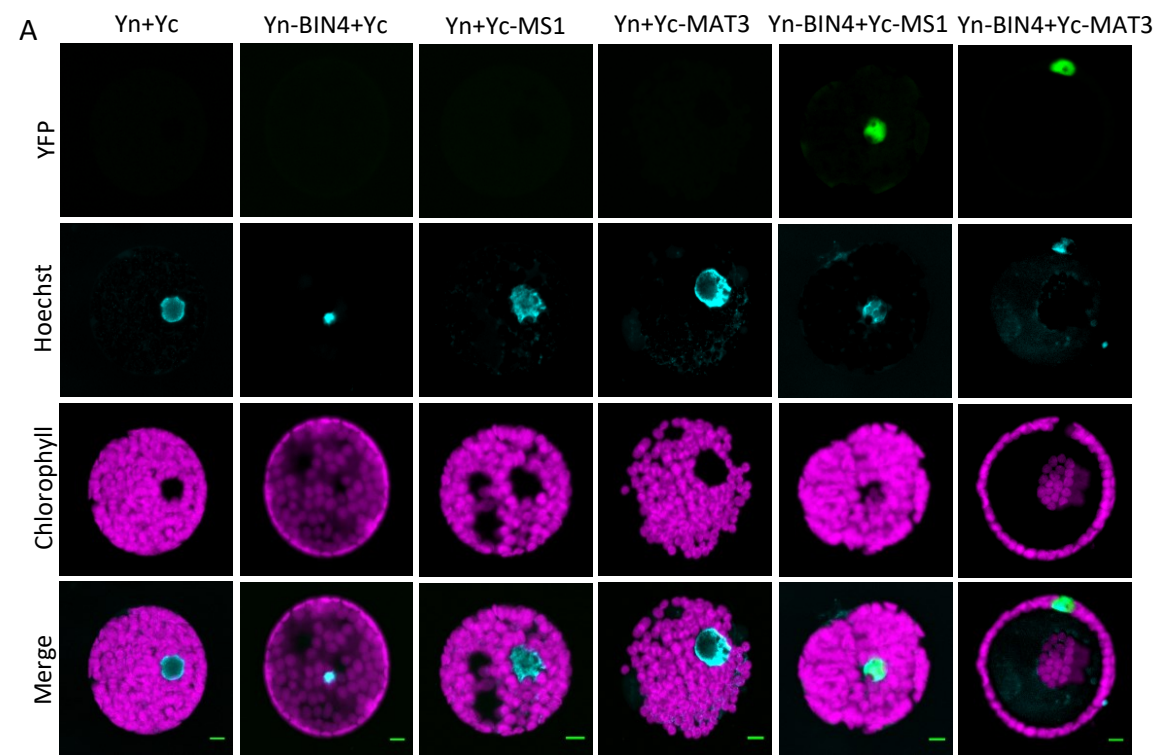


Fig 5

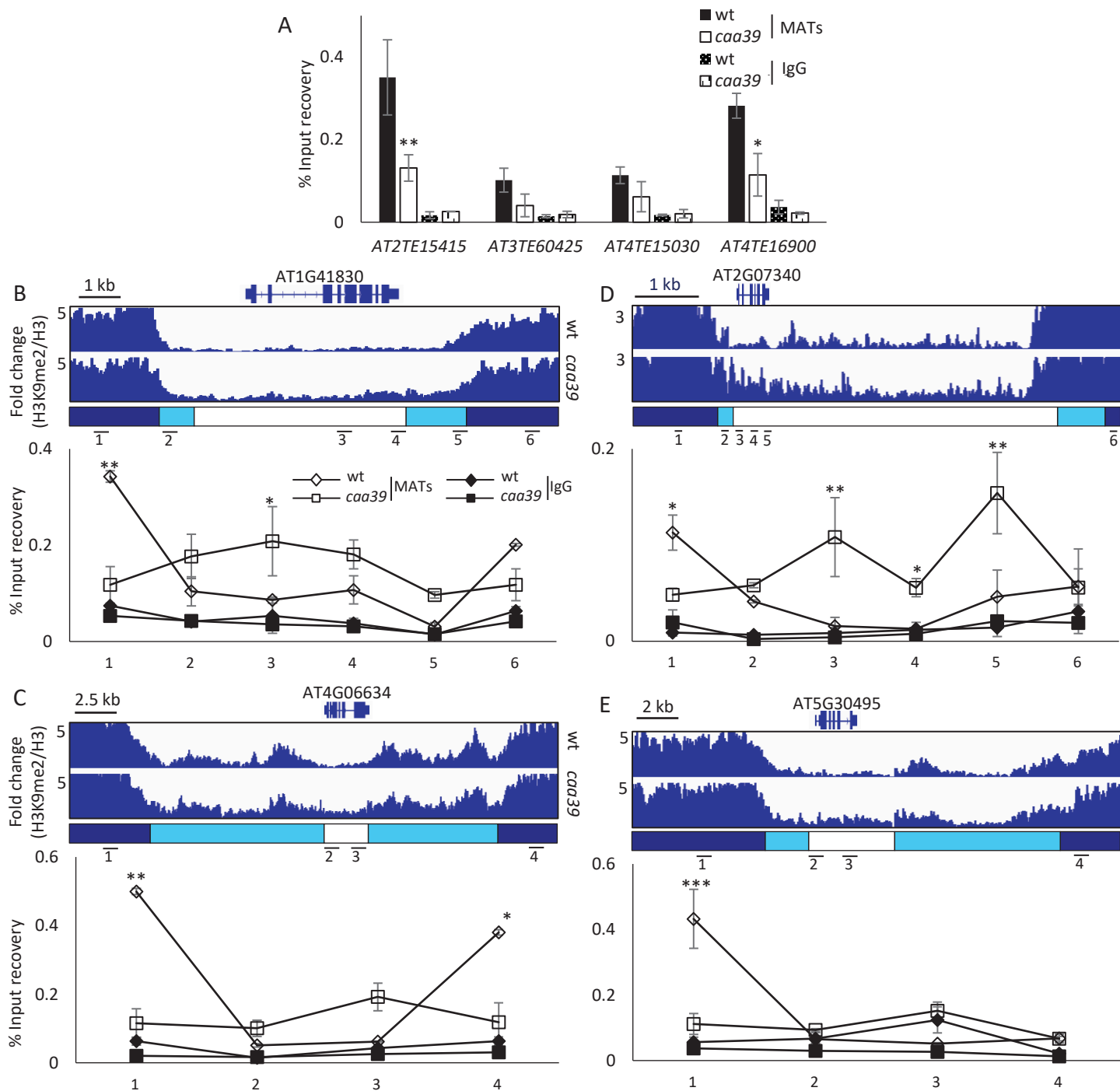


Fig 6